Identification of a Key Ferroptosis-related Gene in Pathogenesis of Gastric Cancer

Shuling Liu
The Second Affiliated Hospital of Soochow University, Soochow University
Mei Huang
Yancheng Third People's Hospital
Chao Li
Yancheng Third People's Hospital
Fujun Shen
Yancheng Third People's Hospital
Chunbin Wang (ycwangchunbin@163.comTel)
Yancheng Third People's Hospital

Research Article

Keywords: FTH1, bioinformatics, gastric cancer, erastin, immune infiltration

Posted Date: May 11th, 2022

DOI: https://doi.org/10.21203/rs.3.rs-1543383/v1

Abstract

Ferroptosis plays a significant role in the development of multiple solid malignancies, including gastric cancer (GC), but largely, physicians still know little about ferroptosis-related genes (FRGs) in GC yet, which require further exploration. In this study, functional enrichment analysis and protein-protein interaction (PPI) analysis were used to analyze the differentially expressed FRGs obtained by RNA sequencing analysis. We then obtained the key gene by intersecting with the ferroptosis database. Thereafter, we performed multi-omics analysis of the key gene using bioinformatics and assessed its effects on tumor proliferation and ferroptosis *in vitro*. We found that FRGs were enriched in biological processes including endocytosis, ribosome, and ferroptosis. The identified key gene ferritin heavy chain 1 (FTH1) was upregulated by erastin treatment in GC cells, and elevated in GC samples compared to normal tissues. And FTH1 expression could discriminate GC from adjacent tissues with a cutoff level of 11.3. Its expression positively correlated with most immune infiltrates, including induced dendric cells, macrophages, and neutrophils, etc. The genetic alteration rate of *FTH1* was 1.36%. The *FTH1* methylation level was high (cg11748881), and patients with *FTH1* hypermethylation had a worse survival. In addition, overexpression of *FTH1* in MGC803 cells promoted GC proliferation and suppressed ferroptosis. FTH1 affects GC development by regulating ferroptosis, providing a new insight for a pharmacological treatment target in GC.

Introduction

Currently, gastric cancer (GC) has a high incidence and mortality worldwide. Although advances in surgery, radiotherapy and chemotherapy have greatly improved the survival rates of patients with gastric cancer, the survival outcomes of those with advanced GC remain unsatisfactory[1]. In search of better treatment options, researchers make great efforts at the molecular level to seek potential treatment targets of GC during its initiation and progression. Accumulating evidence suggests that multiple biological processes such as cell proliferation, apoptosis, and ferroptosis are related to the pathogenesis of GC, among which ferroptosis is particularly critical.

As a novel form of cell death, ferroptosis is characterized by iron accumulation, and accomplished by the participation of multiple metabolites and biomolecules[2]. It’s usually resulted from the disruption of cell membrane integrity related to glutathione peroxidase 4 (GPX4) inactivity as well as lipid peroxides accumulation[3, 4]. However, physicians know little about participation of ferroptosis in the pathogenesis of GC yet, which require further exploration and may provide us with potential intervention targets in GC.

Erastin, a small molecular compound and the most commonly used inducer of ferroptosis, can cause cysteine depletion by inhibiting cystine glutamate antiporter and reducing glutathione (GSH)[5]. We herein profiled differentially expressed genes between erastin-treated and untreated patient derived primary gastric cancer cells using RNA-sequencing (RNA-seq) technique. We then mainly explored the biological processes involving FRGs, as well as expression and epigenetic modification patterns, diagnostic and prognostic prediction performance, and immune infiltration evaluation of key genes therein. Finally, these

bioinformatics-based predictions were fully evaluated and validated *in vitro*. Our findings provide a potential pharmacological therapeutic target for GC based on ferroptosis.

Materials And Methods

RNA-Sequencing

MGC803 cells grown to exponential phase were passaged on average at a 1:2 ratio, one of which was treated with 30 μM erastin while the other was untreated with vehicle control (buffered DMSO). Thereafter, cultures were shaken for 30 min at 37°C prior to total RNA extraction. We performed RNA-seq analysis of the above samples using the Illumina Hiseq X Ten platform (personalbio, Shanghai).

Analysis of Differentially Expressed FRGs

We utilized the “limma” package to determine differentially expressed FRGs at the threshold of |fold change| > 2 and false discovery rate (FDR) < 0.05. Volcano plot and heatmap were generated using the “ggplot2” and “heatmap” packages, respectively.

Functional Enrichment and Protein-Protein Interaction Analysis

We implemented Gene Ontology (GO) and Kyoto Encyclopedia of Genes and Genomes (KEGG) enrichment analyses on differentially expressed gene set using the “ClusterProfiler” package to identify the involved biological pathways. In addition, we framed a visualized protein-protein interaction (PPI) network for the proteins encoded by the differentially expressed FRGs via the STRING webtool (https://STRING-db.org/).

Data Collection

Considering together the FRGs retrieved from our RNA-seq (and differential analysis) versus ferroptosis Regulator & Disease database (FerrDb; http://www.zhounan.org/ferrdb/)[6]. The key gene *FTH1* was obtained in the intersection set. Corresponding single cell RNA and protein expression data were obtained from the Human Protein Atlas (HPA; http://www.proteinatlas.org/)[7].

Considering the small normal sample size in The Cancer Genome Atlas (TCGA; https://genome-cancer.ucsc.edu/) (n = 36), we uniformly downloaded the transcriptome data of normal tissues in the Genotype-Tissue Expression Project (GTEx; http://commonfund.nih.gov/GTEx/)[8] (n = 174) and TCGA tumor tissues (n = 414) from the UCSC Xena platform (https://xenabrowser.net/datapages/). All RNA-seq data processed by Toil[9] were converted to transcripts per kilobase (TPM) format for differential expression analysis of *FTH1* in GC.

Diagnostic Analysis

The diagnostic performance of *FTH1* was assessed by the receiver operating characteristic (ROC) curve, which evaluated the sensitivity and specificity of the diagnostic model. We plotted the curve and assessed the model using the “pROC” and “ggplot2” packages.

Immune Infiltration Estimation

We calculated infiltration scores of 24 immune cell types including activated DCs, B cells, CD8 T cells, etc. using the single sample Gene Set Enrichment Analysis (ssGSEA) algorithm built into the “gene set variation analysis (GSVA)” package to evaluate the immune infiltration landscape[10].

Analysis of Mutation and DNA Methylation

We obtained data of genetic alterations in tumor tissues using the cBioPortal database (https://www.cbioportal.org/). To gain further insight into epigenetic modifications, we used MethSurv©2017 (https://biit.cs.ut.ee/methsurv/)[11] to interrogate DNA methylation alterations via “single CpG” and “Gene visualization” panels.

Cell Culture

The human GC cell line MGC-803 and normal gastric mucosa cell line GES-1 were purchased from the Chinese Academy of Sciences (Shanghai, P.R. China). Both were cultured in Dulbecco Modified Eagle Medium (DMEM) supplemented with 10% fetal bovine serum (FBS), 1000 U/mL penicillin, and 100 mg/mL streptomycin (Hyclone, USA) at 37°C with 5% CO2.

Real-time Quantitative Polymerase Chain Reaction (qRT-PCR)

Total RNA was extracted using RNAiso Plus (TaKaRa, Japan) and then reverse transcribed into cDNA using a TaKaRa Kit (Qiagen, Japan) according to the manufacturer's instructions. Real time PCR was performed to detect the mRNA levels of FTH1 using a QuantiNova SYBR Green PCR Kit (Qiagen, Hamburg, Germany). Glyceraldehyde-3-phosphate dehydrogenase (GAPDH) was set as an internal reference. Primers were designed and synthesized by Anhui General Co., Ltd. using the Primer-Blast online-based software. The primers sequences are listed as follows: FTH1: F: 5’-CCCCCATTTGTGTGACTTCAT-3’, R: 5’-GCCCGAGGCTTAGCTTTCATT-3’. GAPDH: F: 5’-ATGTTCGTCATGGGTGTGAAC-3’, R: 5’-ATGGACTGTGGTCATGAGTCC-3’. We used the ABI Prism 7500 SDS Software to analyze the qRT-PCR results.

Over-expression of FTH1

Plasmid vectors (generalbiol, Anhui, China) were transfected into MGC803 cells to overexpress *FTH1* (OE-FTH1), while empty vector pcDNA3.1-EGFP was used as a control. In brief, 50 μL of Lipofectamine 2000 (Invitrogen 11668030) and plasmids were diluted in high glucose DMEM (Hyclone SH30243.01B), mixed, and then incubated in the dark for 15 minutes. The resulted mixture was applied to MGC803 cells and incubated for 6 hours. Finally, we used qRT-PCR to validate transfection efficiency, and the cells with *FTH1* overexpression were cultured for further study.

MTT Assay

Cell proliferation was detected by MTT assay. Specifically, transfected cells were seeded into 96 well plates containing 10 μL MTT solution and incubated under normal culture conditions for 4 hours. Then, we removed the MTT solution and added dimethyl sulfoxide (DMSO) to dissolve the formazan crystals. The optical density (OD) value was measured at 492 nm with a microplate reader (Bio-tek ELX800, Winooski, VT) to represent cell viability.

Lipid Peroxidation and Glutathione Measurements

Oxidative stress was quantified with lipid reactive oxygen species (ROS) levels, whereas lipid peroxidation was assessed using malondialdehyde (MDA) content. Iron-dependent ROS accumulation based on toxic lipids is a key contributing factor within ferroptosis[12, 13]. Cellular ROS production was evaluated by fluorescence generated from the oxidation of the intracellular probe 2,7-dichlorodihydrofluorescein diacetate (DCFH-DA) using a commercial kit (Beyotime, S0033S). Cells were imaged under a fluorescent inverted microscope (OLYMPUS, IX71) at an excitation wavelength of 488 nm and an emission wavelength of 525 nm. MDA produced after oxidation of biological membranes is the end product of lipid peroxidation, whose concentration in cell lysates was detected by an MDA kit (Nanjing Jiancheng, A003-1-1) at 532 nm. Glutathione (GSH) levels were measured using a GSH assay detection kit (Ybio, YB-GSH-Hu) at 450 nm following the manufacturer's instructions.

Statistical Analysis

Two-sided student's t test was used to compare the means of two groups, while one-way analysis of variance was used to compare multiple groups. Data were analyzed using GraphPad Prism 7.0 (San Diego, CA) and R software (version 3.3.2). Data were considered statistically significant as follows, * $p < 0.05$, ** $p < 0.01$, or *** $p < 0.001$.

Results

Differentially Expressed FRGs Were Identified Using RNA-seq

The flow chart of our analysis is presented as Fig. 1. Following the pre-specified thresholds, we obtained a differentially expressed gene set (n = 69; 53 upregulated and 16 downregulated genes) by RNA-seq as well as differential analysis between erastin-treated and untreated groups (Fig. 2A; Table S1). The heatmap of FRGs based on hierarchical clustering indicated that the expression patterns of differentially expressed genes could be well discerned after unsupervised clustering (Fig. 2B).

Functional Enrichment and PPI Analysis of FRGs

Gene ontology enrichment analysis of FRGs between erastin-treated and untreated gastric cancer cells indicated that most of them were enriched in the extracellular exosomes, and participating in the molecular functions of GTPase activity. From the viewpoint of biological process (BP), phylloquinone metabolic process was the most significantly enriched term for FRGs (Fig. 3A). Meanwhile, the differentially expressed FRGs were confirmed to be enriched in several KEGG pathways related to endocytosis, ribosome, and ferroptosis (Fig. 3B).

To determine the interactions among protein products encoded by the differentially expressed FRGs, we performed PPI analysis. The resulted interactions are shown in detail in Fig. 4A-B. Notably, UBB was the node sharing the largest number of interactions across these differentially expressed FRGs.

Identification of FTH1 and Its Expression Pattern

The key gene *FTH1* was then obtained by intersecting the differentially expressed gene set with the FRGs extracted from the ferroptosis database. Thereafter, we carried out a set of bioinformatics analyses and biological experiments to validate our screening and prediction results.

Using the HPA database to analyze *FTH1* expression pattern in normal cells, we found that it was mainly enriched in blood and immune cell types, including Langerhans cells, monocytes, and proximal enterocytes (Fig. 5A). Furthermore, we examined the expression pattern of FTH1 protein in 44 normal samples. It was expressed in low or undetectable amounts in most tissues, including gastric glandular cells, to a moderate extent in tissues such as pancreas and kidney, while highly expressed in cerebral cortex and bone marrow tissues (Fig. 5B).

Next, we retrieved the differential expression pattern of *FTH1* in cancer tissues versus adjacent normal tissues in pan-cancer (n = 33) and observed that the mRNA levels of *FTH1* in most solid tumors were generally elevated compared to those in normal controls (Fig. 5C).

Differential Expression of FTH1 in Normal and Gastric Cancer Samples

We compared FTH1 mRNA expression between 414 GC samples and 210 normal tissue samples (36 from TCGA-STAD cohort and 174 from GTEx). As shown in Fig. 6A, *FTH1* was significantly upregulated in GC tissues ($P < 0.001$). To further determine the significance of the biological function of FTH1 at the protein level, we accessed a cohort (containing 354 cases of primary GC paired with non-cancerous tissues) that underwent immunohistochemical staining in HPA. Consistent with the RNA pattern, the FTH1 protein was stained at a low level in normal gastric glandular tissues but at a significantly elevated level in GC tissues. Representative images are shown in Fig. 6B. In addition, we carried out ROC to estimate the discrimination efficacy of FTH1 between GC and corresponding normal tissues. The AUC for *FTH1* was 0.619, 95% confidence interval (95%CI) 0.573 to 0.664 (Fig. 6C), suggesting that *FTH1* might be an identifying biomarker for GC.

Correlations of FTH1 Expression and Immune Infiltration

Next to investigate the immunomodulatory role of FTH1, we assessed the relationship between *FTH1* expression and immune infiltration level in GC samples. The results of correlation analyses of FTH1 with immune cells are shown in Table 1. and Fig. 7, the *FTH1* expression level in GC showed a positive correlation with the infiltration of most immune cells. Taken together, these findings suggested that FTH1 might influence immune cell infiltration in GC.

Genetic Alteration and DNA Methylation of FTH1 in Gastric Cancer

Different degrees of genetic alterations in *FTH1* were detected in 25 of 32 cancer types, including mutations, amplifications, deep deletions, and multiple alterations (Fig. 8A). Detailed mutations in *FTH1* are shown in Fig. 8B, and we found that the genetic alteration rate was 1.36% among the 440 sequenced GC samples.

In addition, we presented the annotation information of DNA methylation probes and samples with a heatmap, including CpG sites, genomic regions, relation to islands, age, body mass index (BMI), ethnicity, survival status, etc. Through visualization of methylation levels and *FTH1* expressions, we found that *FTH1* methylation level was high in cg11748881 probe (Fig. 9A), and patients with *FTH1* hypermethylation had a poor overall survival. Meanwhile, we found that 3 CpG sites (cg24898753, cg24496614, and cg09367425) located in CpG islands indicated a better prognosis (Fig. 9B-D).

Figure 9 The MethSurv obtained the effect of methylation level and FTH1 expression on prognosis in GC. (A) The visualization between the methylation level and the FTH1 expression; (B–D) the Kaplan–Meier survival of the promoter methylation of FTH1

The Mechanism of FTH1 on Erastin-induced Ferroptosis in GC

By suppressing cystine uptake by cells, erastin increases GSH depletion and inactivates GPX4, which leads to the accumulation of lipid peroxidation, resulting in ferroptosis[14]. A study has shown that cellular sensitivity to ferroptosis is related to multiple biological pathways, including lipid, glutathione, and iron metabolism[15]. As shown in Fig. 10, *FTH1* was involved in iron storage and autolysosomes and contributed to the maintenance of iron homeostasis and protection against iron overload.

FTH1 Overexpression Promoted Proliferation and Blocked Ferroptosis

To elucidate the role of *FTH1* in GC pathogenesis, we transfected MGC803 cells with plasmid vectors to overexpress *FTH1 in vitro*, and RT-qPCR verified that the transfection efficiency was high (Fig. 11A). *FTH1* overexpression promoted the proliferation of MGC803 cells (Fig. 11B). GSH/GPX4-based ROS scavenging

indispensably prevents lipid peroxidation during ferroptosis[16]. GSH levels were increased in OE-FTH1 cells (Fig. 11C). *FTH1* overexpression inhibited ROS generation and MDA production (Fig. 11D-F).

Discussion

Accumulating evidence suggests that ferroptosis is important within GC development[17–19]. Yet, the key FRGs there remain undefined and require further extensive exploration to improve the understanding of ferroptosis in GC pathogenesis. Our study identified FRGs of GC and further investigated the mechanisms of ferroptosis in GC. We obtained 69 differentially expressed genes in gastric cancer cells treated by a ferroptosis inducer, which interacted with each other and were involved in biological processes including endocytosis, ribosome and ferroptosis.

Importantly, we took the intersection of differentially expressed genes and FRGs accessed from the ferroptosis dataset to obtain *FTH1*, which was confirmed to be in a high expression level in tumor tissues with promise as a diagnostic marker using multiple online tools. The *FTH1* mRNA level in GC was positively correlated with most immune cells as well as DNA methylation, and the overall survival of patients carrying FTH1 hypermethylation was poor. *In vitro* experiments demonstrated that *FTH1* overexpression in MGC803 cells Inhibited ferroptosis and promoted GC proliferation, suggesting that FTH1 is a key regulatory molecule of ferroptosis in gastric cancer and holds promise as a therapeutic target.

To our knowledge, there is some published literature exploring FRGs in cancer[20–23]. FRG-based risk models were previously suggested to accurately predict prognosis in clear cell renal cell carcinoma[24]. Interestingly, our PPI results suggested multiple interactions for UBB (Ubiquitin B), ribosomal protein S27 (RPS27), and FTH1. We know that high UBB expression predicts worse prognosis in non-smokers with lung adenocarcinoma[25], RPS27 correlated with unfavorable OS in patients with triple-negative breast cancer [26], and FTH1 disruption inhibits growth and tumorigenesis in certain molecular subtypes of breast cancer[27]. Similar to previous studies, our study reveals that the novel FRG signature may predict poor prognosis and modulate cell proliferation, which facilitates personalized therapy.

More plausible explanations are obtained when we direct our eye to the molecular level. Ferritin, consisting of ferritin heavy and ferritin light chains, is highly conserved and widely expressed. Its heavy chain (encoded by FTH1) catalyzes the oxidation reaction of Fe^{2+}, whereas ferritin light chain is vital for ferric iron (Fe^{3+}) storage[28]. Mohamed et al. demonstrated that estrogen-induced *FTH1* methylation inhibited hepatocarcinogenesis[29]. Meanwhile, FTH1 was proposed to be associated with lymph node metastasis and distant metastasis[30], as well as macrophage abundance in head and neck squamous cell carcinoma[12]. Consistently, we observed in gastric cancer that *FTH1* expression was tightly correlated with DNA methylation and positively correlated with most immune cells, with *FTH1* hypermethylation indicating worse overall survival. Moreover, overexpression of *FTH1* in MGC803 cells promoted GC proliferation and suppressed ferroptosis, providing evidence to support FTH1 functions as a promising therapeutic target for GC.

However, one disadvantage is that we only validated the expression level of FRGs in vitro, but did not study the potential mechanism of the FRGs in mouse models or in clinical samples. Therefore, further studies are need in future.

Conclusion

Combining the experimentally obtained differentially expressed genes with data from public databases, we identified *FTH1*, as a key gene which may affect GC development by regulating ferroptosis, providing new insights into personalized treatment for patients with gastric cancer .

Abbreviations

gastric cancer: GC; ferroptosis-related genes: FRGs; protein-protein interaction: PPI; key gene ferritin heavy chain 1: FTH1; glutathione peroxidase 4 : GPX4; glutathione: GSH; Gene Ontology: GO); Kyoto Encyclopedia of Genes and Genomes: KEGG.

Declarations

Ethics approval and consent to participate

The database is freely accessible and available and therefore there was no need to get approval from the local ethics committee.

Consent to publish

Not applicable.

Availability of data and materials

The raw data supporting the conclusions of this article will be made available by the authors, without undue reservation.

Competing interests

The authors declare no competing interests.

Funding

The authors received no funding for this work.

Acknowledgement

We would like to thank researchers and staff working for TCGA, GTEx, String, cBioPorta, MethSurv, etc.

Authors Contribution

Shuling Liu drafted the manuscript. Chunbin Wang designed experiments, participated in coordination, and critically revised the manuscript. Mei Huang, Chao Li and Fujun Shen analyzed data. All authors contributed to the article and approved the submitted version.

References

1. Sorup S, Darvalics B, Khalil AA, Nordsmark M. Haee M et al. Treatment and Survival in Advanced Non-Small Cell Lung Cancer, Urothelial, Ovarian, Gastric and Kidney Cancer: A Nationwide Comprehensive Evaluation. Clin Epidemiol 2021;13:871-882.
2. Chen X, Comish PB, Tang D. Kang R. Characteristics and Biomarkers of Ferroptosis. Front Cell Dev Biol 2021;9:637162.
3. Fujii J, Homma T. Kobayashi S. Ferroptosis caused by cysteine insufficiency and oxidative insult. Free Radic Res 2020;54:969-980.
4. Yang WS. Stockwell BR. Ferroptosis: Death by Lipid Peroxidation. Trends Cell Biol 2016;26:165-176.
5. Chen D, Fan Z, Rauh M, Buchfelder M. Eyupoglu IY et al. ATF4 promotes angiogenesis and neuronal cell death and confers ferroptosis in a xCT-dependent manner. Oncogene 2017;36:5593-5608.
6. Zhou N. Bao J. FerrDb: a manually curated resource for regulators and markers of ferroptosis and ferroptosis-disease associations. Database (Oxford) 2020;2020.
7. Uhlen M, Fagerberg L, Hallstrom BM, Lindskog C. Oksvold P et al. Proteomics. Tissue-based map of the human proteome. Science 2015;347:1260419. http://doi.org/10.1126/science.1260419
8. Consortium G. The Genotype-Tissue Expression (GTEx) project. Nat Genet 2013;45:580-5.
9. Vivian J, Rao AA, Nothaft FA, Ketchum C. Armstrong J et al. Toil enables reproducible, open source, big biomedical data analyses. Nat Biotechnol 2017;35:314-316.
10. Hanzelmann S, Castelo R. Guinney J. GSVA: gene set variation analysis for microarray and RNA-seq data. Bmc Bioinformatics 2013;14:7.
11. Metsalu T. Vilo J. ClustVis: a web tool for visualizing clustering of multivariate data using Principal Component Analysis and heatmap. Nucleic Acids Res 2015;43:W566-70.
12. Tang D, Chen X, Kang R. Kroemer G. Ferroptosis: molecular mechanisms and health implications. Cell Res 2021;31:107-125.
13. Stockwell BR, Jiang X. Gu W. Emerging Mechanisms and Disease Relevance of Ferroptosis. Trends Cell Biol 2020;30:478-490.
14. Yang WS, SriRamaratnam R, Welsch ME, Shimada K. Skouta R et al. Regulation of ferroptotic cancer cell death by GPX4. Cell 2014;156:317-331.

15. Stockwell BR, Friedmann AJ, Bayir H, Bush AI. Conrad M et al. Ferroptosis: A Regulated Cell Death Nexus Linking Metabolism, Redox Biology, and Disease. Cell 2017;171:273-285.
16. Yang WS, SriRamaratnam R, Welsch ME, Shimada K. Skouta R et al. Regulation of ferroptotic cancer cell death by GPX4. Cell 2014;156:317-331.
17. Fonseca-Nunes A, Agudo A, Aranda N, Arija V. Cross AJ et al. Body iron status and gastric cancer risk in the EURGAST study. Int J Cancer 2015;137:2904-14.
18. Xiao S, Liu X, Yuan L. Wang F. A Ferroptosis-Related lncRNAs Signature Predicts Prognosis and Therapeutic Response of Gastric Cancer. Front Cell Dev Biol 2021;9:736682.
19. Liu SJ, Yang YB, Zhou JX, Lin YJ. Pan YL et al. A Novel Ferroptosis-Related Gene Risk Signature for Predicting Prognosis and Immunotherapy Response in Gastric Cancer. Dis Markers 2021;2021:2385406.
20. Ye Y, Dai Q, Li S, He J. Qi H. A Novel Defined Risk Signature of the Ferroptosis-Related Genes for Predicting the Prognosis of Ovarian Cancer. Front Mol Biosci 2021;8:645845.
21. Zhou J, Wang X, Li Z. Jiang R. Construction and analysis of a novel ferroptosis-related gene signature predicting prognosis in lung adenocarcinoma. Febs Open Bio 2021;11:3005-3018.
22. Liu G, Ma JY, Hu G. Jin H. Identification and validation of a novel ferroptosis-related gene model for predicting the prognosis of gastric cancer patients. Plos One 2021;16:e0254368.
23. Weijiao Y, Fuchun L, Mengjie C, Xiaoqing Q. Hao L et al. Immune infiltration and a ferroptosis-associated gene signature for predicting the prognosis of patients with endometrial cancer. Aging (Albany NY) 2021;13:16713-16732.
24. Wu G, Wang Q, Xu Y, Li Q. Cheng L. A new survival model based on ferroptosis-related genes for prognostic prediction in clear cell renal cell carcinoma. Aging (Albany NY) 2020;12:14933-14948.
25. Deng H, Huang Y, Wang L. Chen M. High Expression of UBB, RAC1, and ITGB1 Predicts Worse Prognosis among Nonsmoking Patients with Lung Adenocarcinoma through Bioinformatics Analysis. Biomed Res Int 2020;2020:2071593.
26. Lin Z, Peng R, Sun Y, Zhang L. Zhang Z. Identification of ribosomal protein family in triple-negative breast cancer by bioinformatics analysis. Biosci Rep 2021;41.
27. Ali A, Shafarin J, Unnikannan H, Al-Jabi N. Jabal RA et al. Co-targeting BET bromodomain BRD4 and RAC1 suppresses growth, stemness and tumorigenesis by disrupting the c-MYC-G9a-FTH1axis and downregulating HDAC1 in molecular subtypes of breast cancer. Int J Biol Sci 2021;17:4474-4492.
28. Friedman A, Arosio P, Finazzi D, Koziorowski D. Galazka-Friedman J. Ferritin as an important player in neurodegeneration. Parkinsonism Relat Disord 2011;17:423-30.
29. Muhammad JS, Bajbouj K, Shafarin J. Hamad M. Estrogen-induced epigenetic silencing of FTH1 and TFRC genes reduces liver cancer cell growth and survival. Epigenetics-Us 2020;15:1302-1318.
30. Huang H, Qiu Y, Huang G, Zhou X. Zhou X et al. Value of Ferritin Heavy Chain (FTH1) Expression in Diagnosis and Prognosis of Renal Cell Carcinoma. Med Sci Monit 2019;25:3700-3715.

Tables

Table 1 and table S1 are not available with this version

Figures

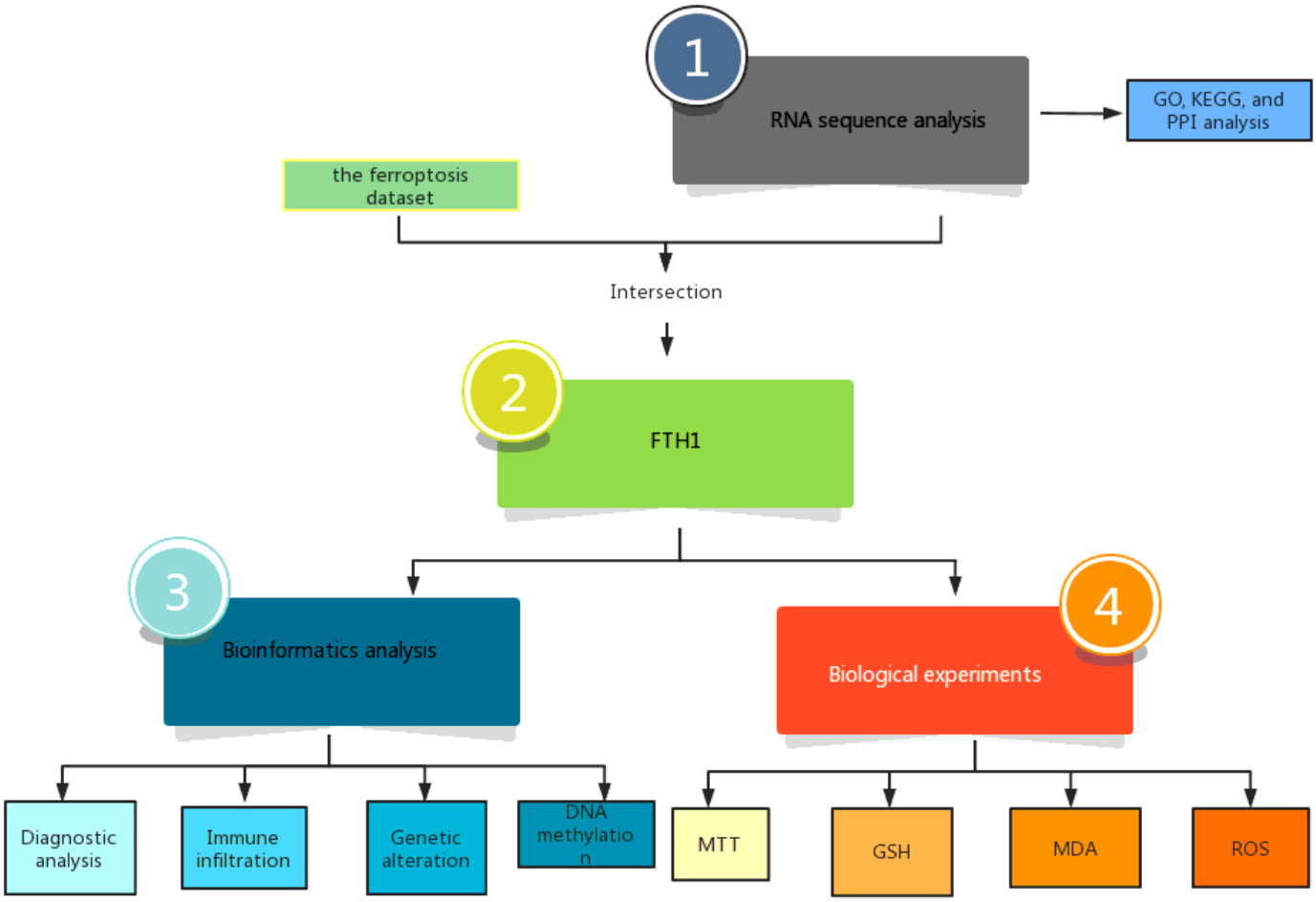

Figure 1

The visual flow-process diagram of this study

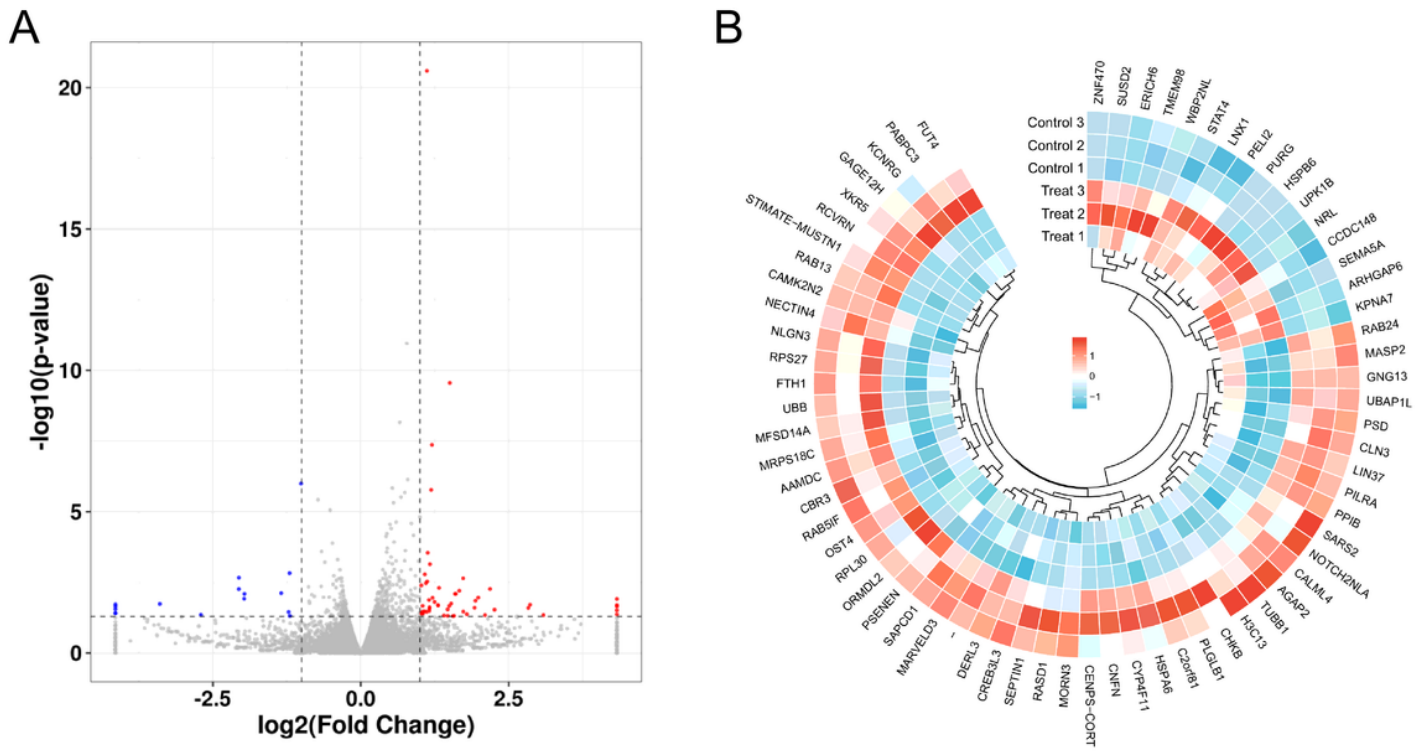

Figure 2

Differentially expression of FRGs. (A)Volcano plot of differentially expression genes between erastin-treated and non-treated samples. (B) Heatmap of the 69 differentially expressed FRGs.

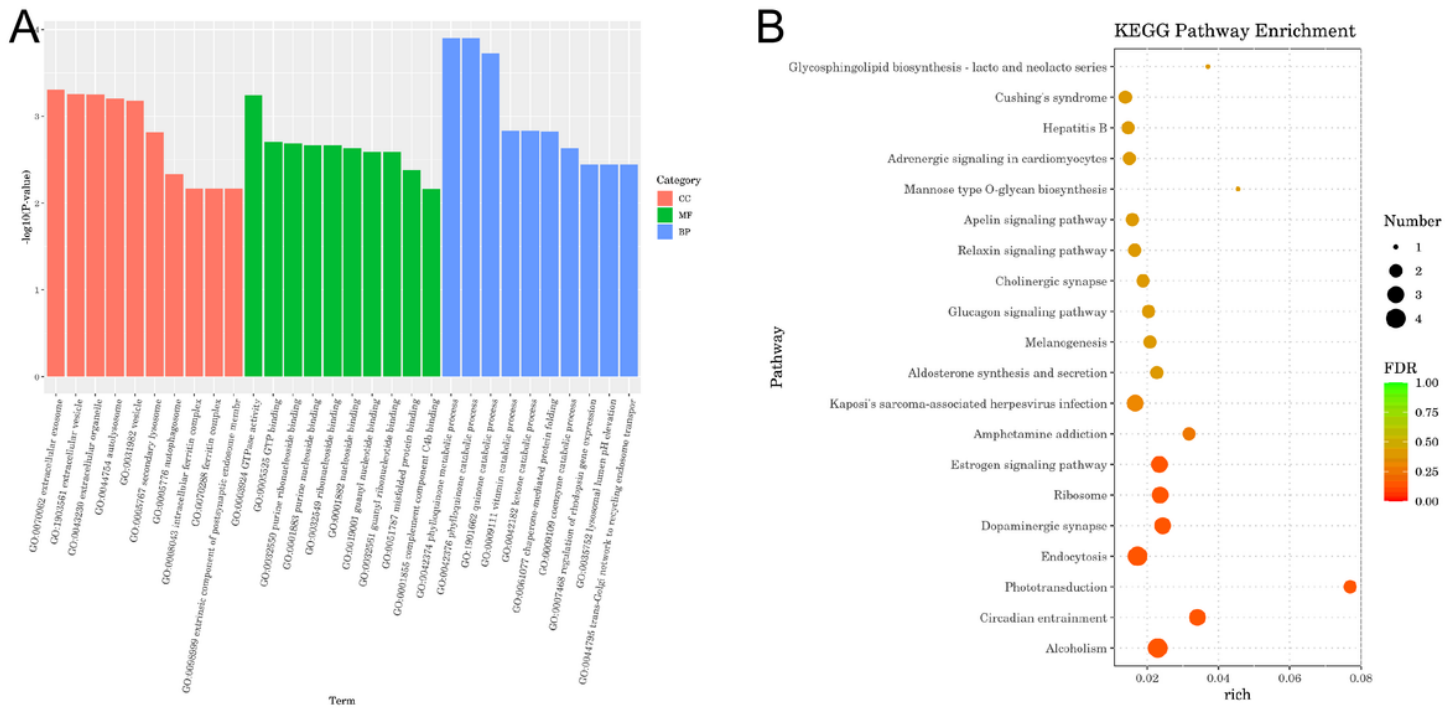

Figure 3

GO and KEGG enrichment analysis

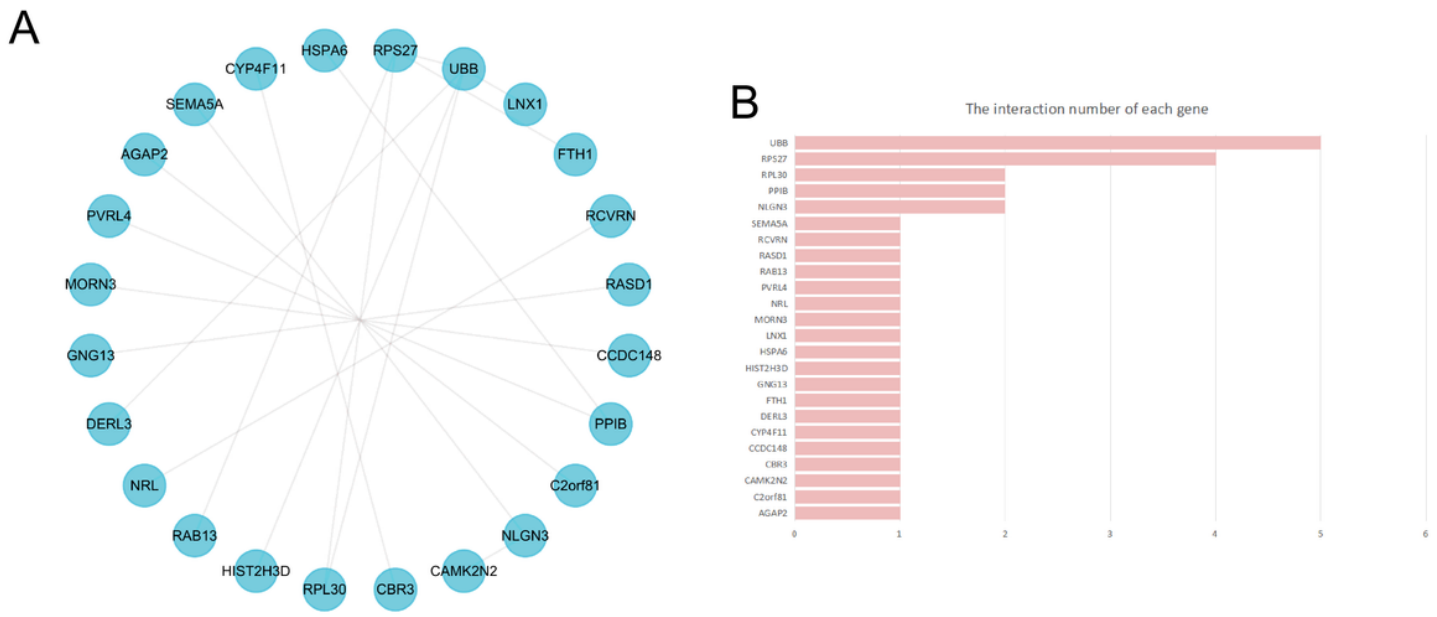

Figure 4

Protein–protein interactions (PPI) analysis the differentially expressed FRGs. (A) The PPI among 69 differentially expressed FRGs. (B) The interaction number of each differentially expressed FRG.

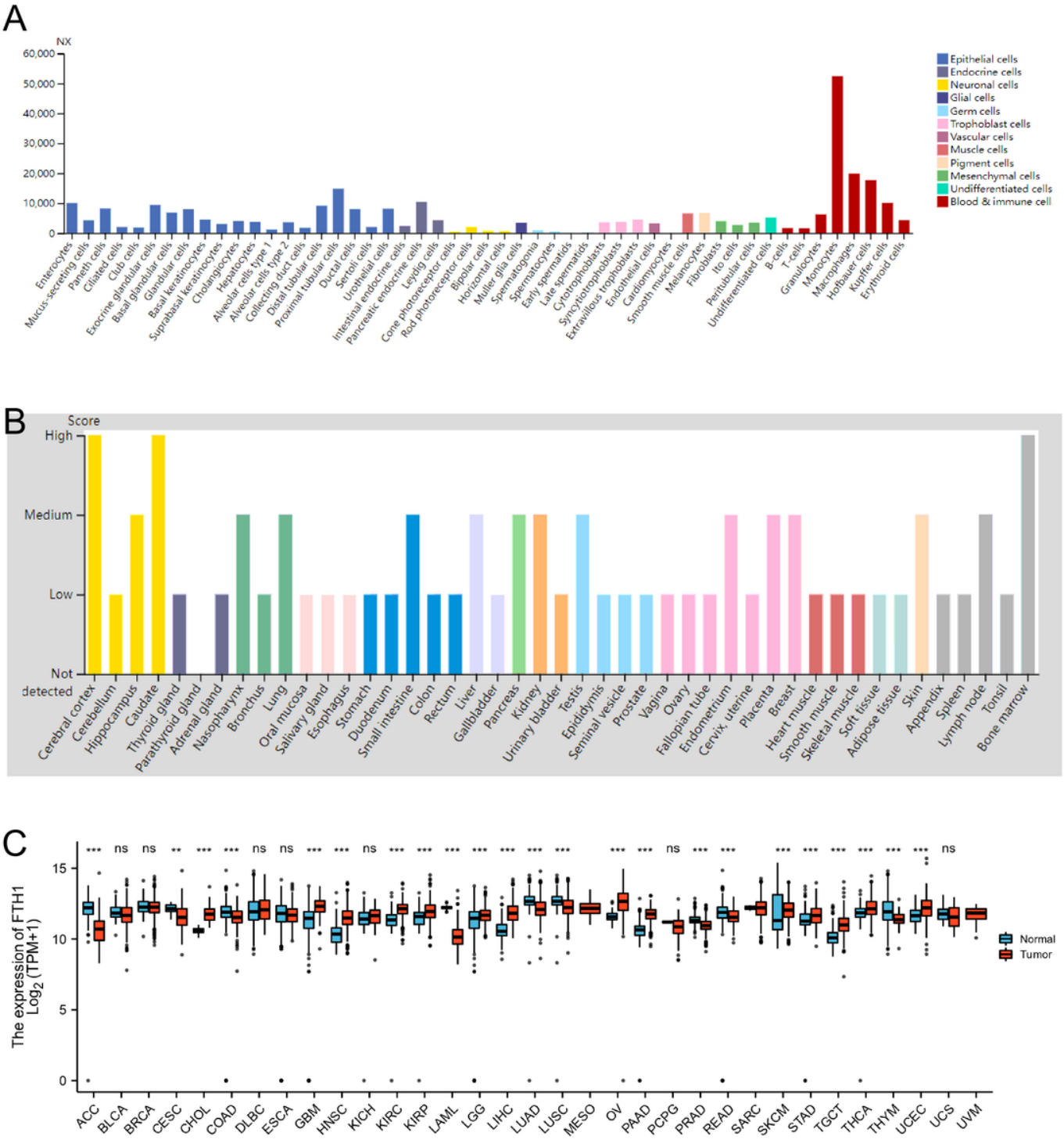

Figure 5

FTH1 expression in pan-cancer. (A) A summary of single cell RNA from all single cell types. Color-coding is based on cell type groups, each consisting of cell types with functional features in common. (B) Protein expression data is shown for each of the 44 tissues. Color-coding is based on tissue groups, each consisting of tissues with functional features in common. (C) Expression pattern of FTH1 in pan-cancer.

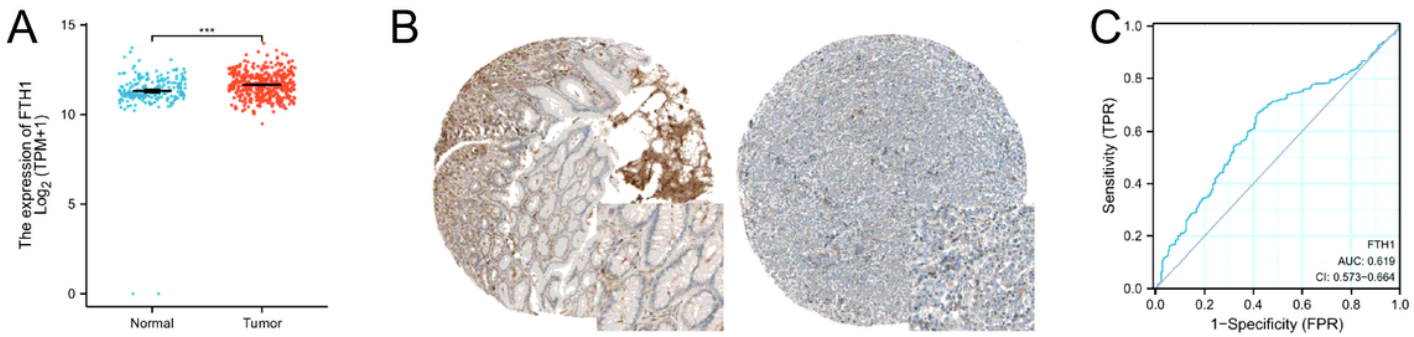

Figure 6

Differentially expression and ROC of FTH1 in normal and gastric cancer samples . (A)mRNA Expression of FTH1 was derived from TCGA-GTEx-STAD. (B) Protein expression of FTH1 was derived from HPA. (C) ROC of FTH1 in GC.

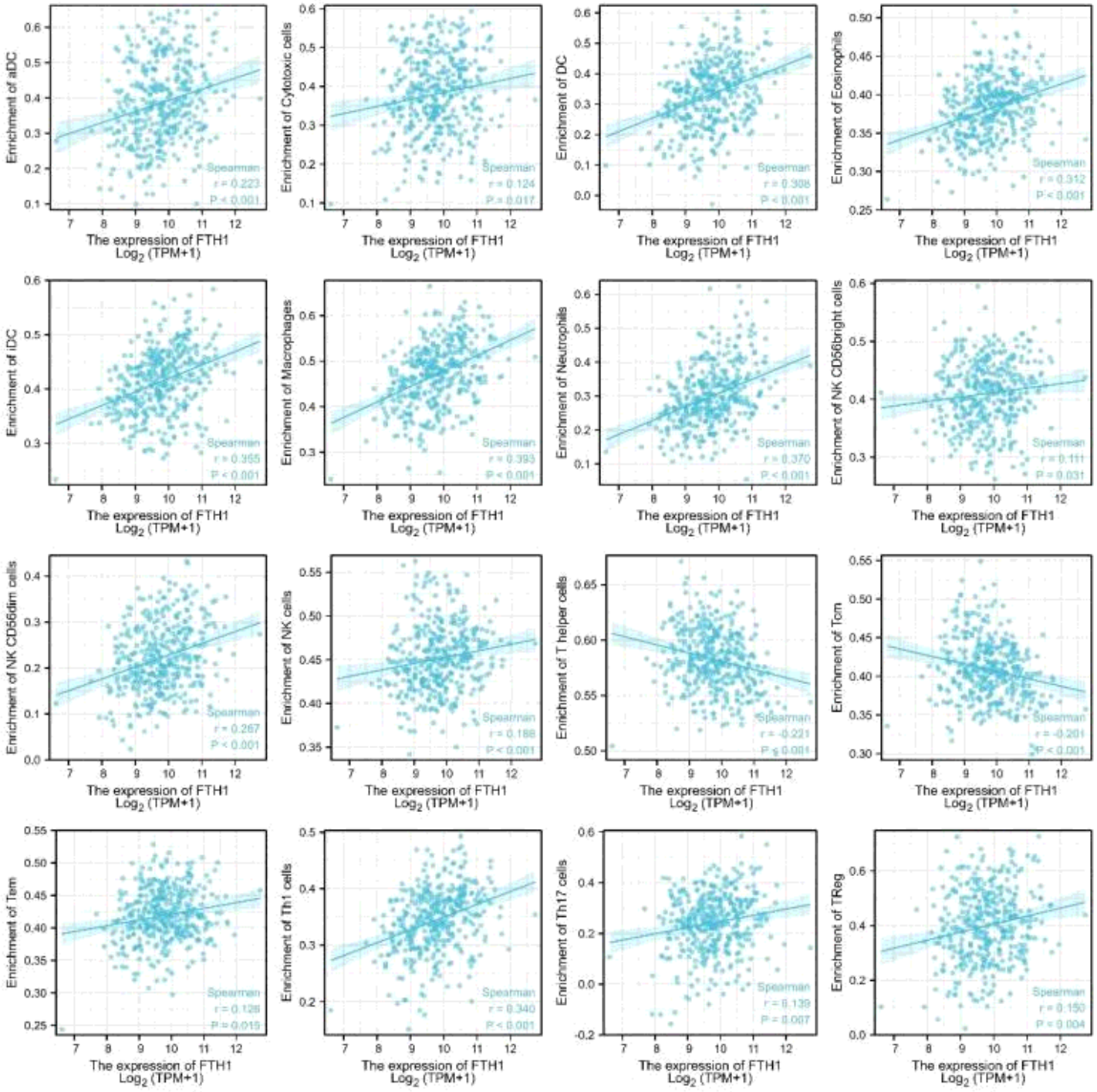

Figure 7

Correlations of FTH1 expression and immune cell (aDC , Macrophages, iDC, Eosinophils, Neutrophils, DC, Mast cells, Tem, Tcm, Helper cells, CD56dim cells, Th1 cells, NK cells, TReg and Th17 cells,) infiltration.

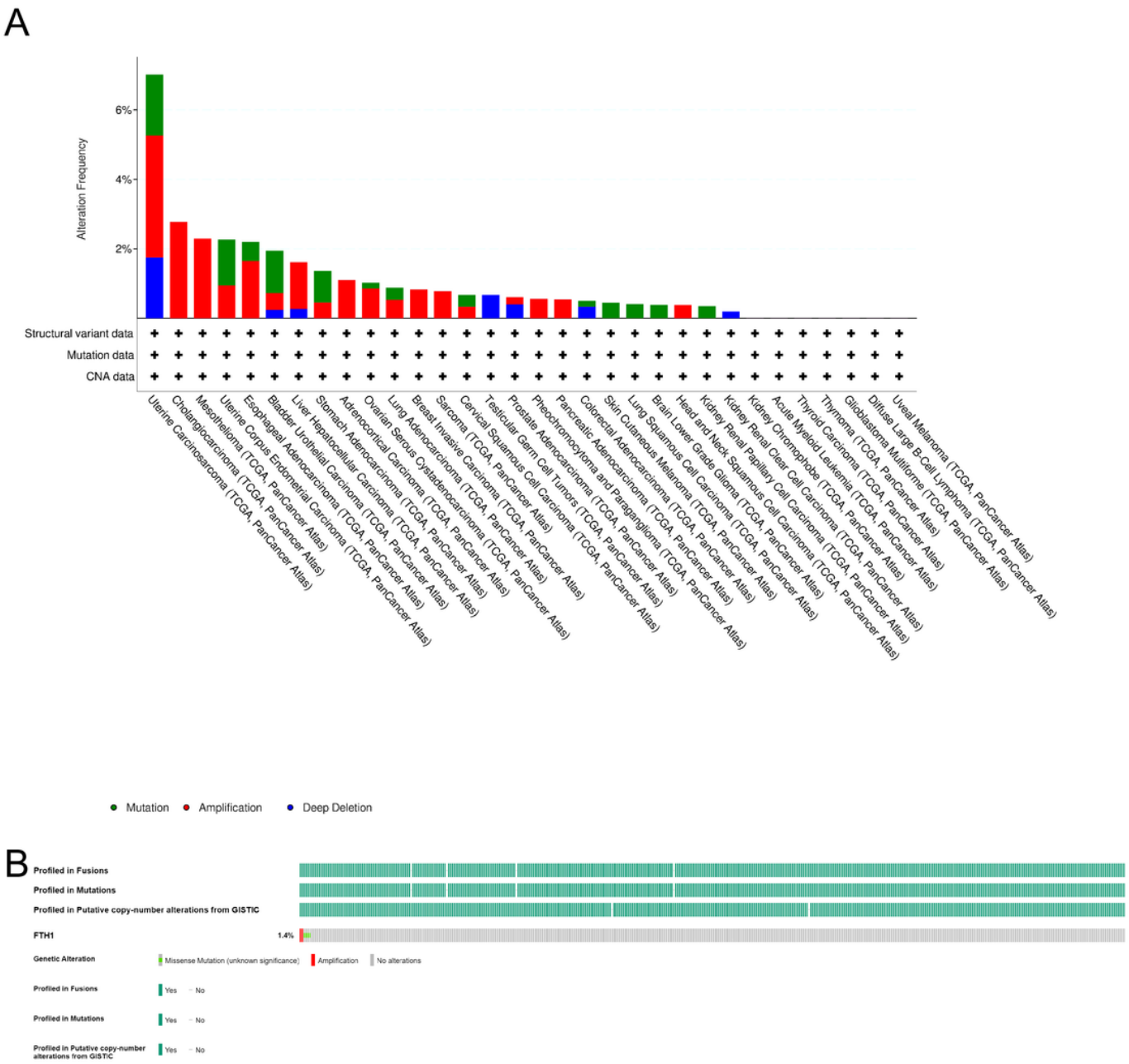

Figure 8

The gene alteration of FTH1. (A)The gene alteration of FTH1 in pan-cancer; (B)The gene alteration of FTH1 in GC. each bar represents one patient.

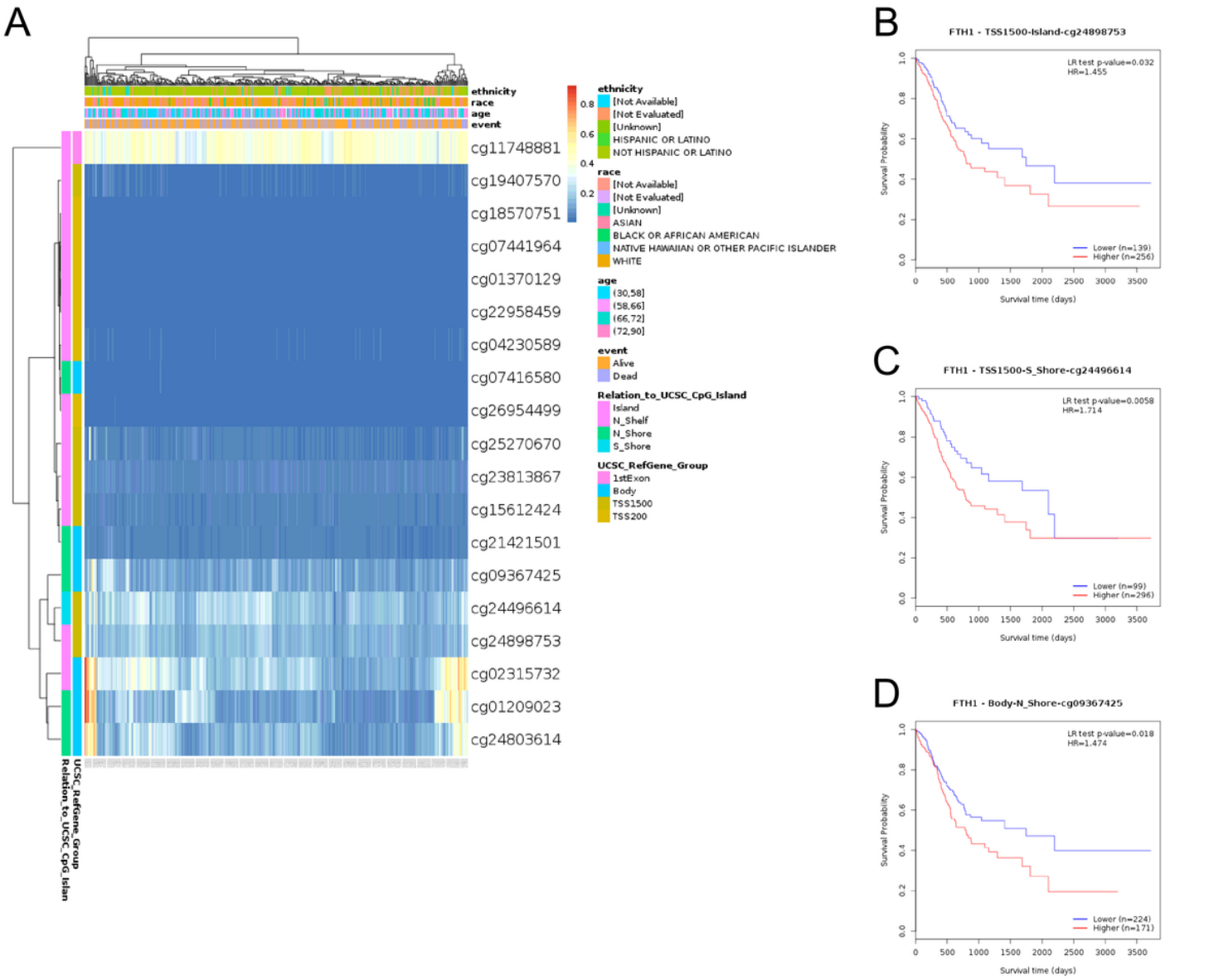

Figure 9

The MethSurv obtained the effect of methylation level and FTH1 expression on prognosis in GC. (A) The visualization between the methylation level and the FTH1 expression; (B–D) the Kaplan–Meier survival of the promoter methylation of FTH1

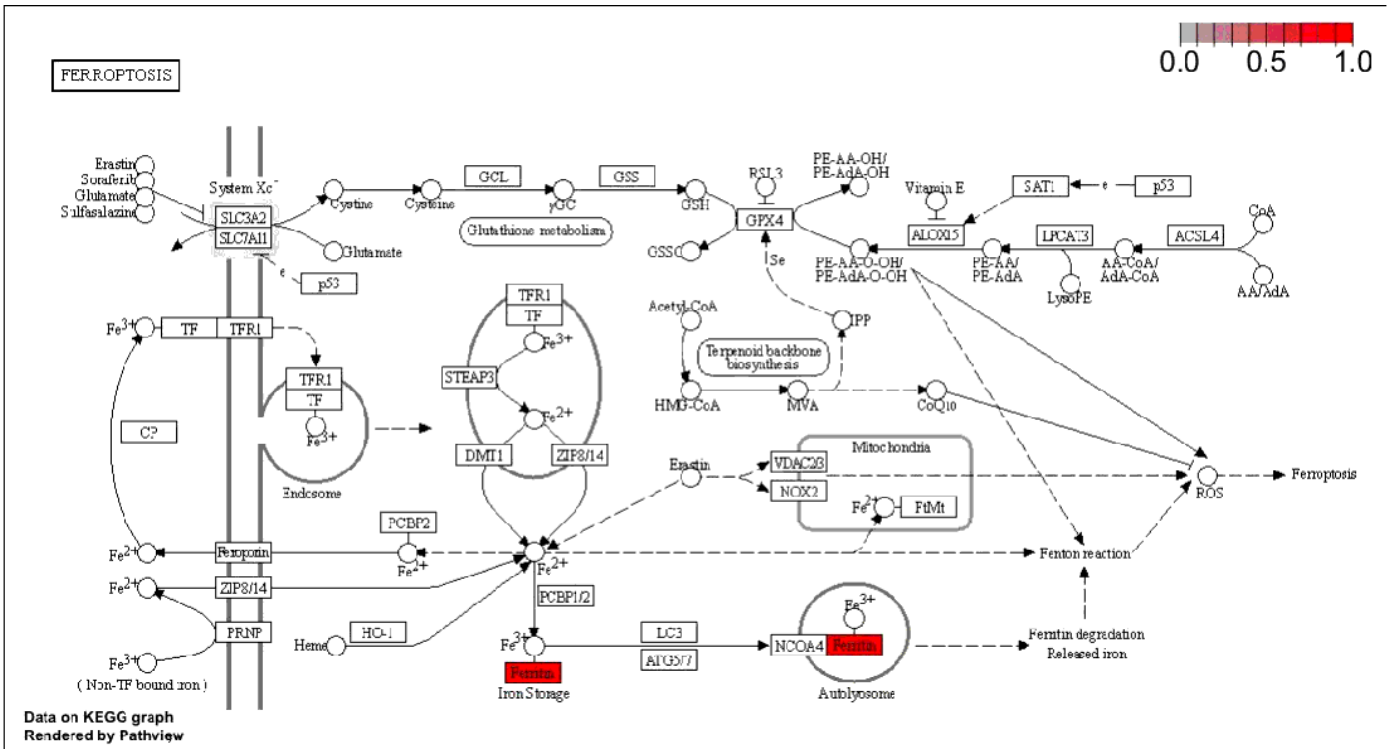

Figure 10

Ferroptosis signaling pathway associated with FTH1

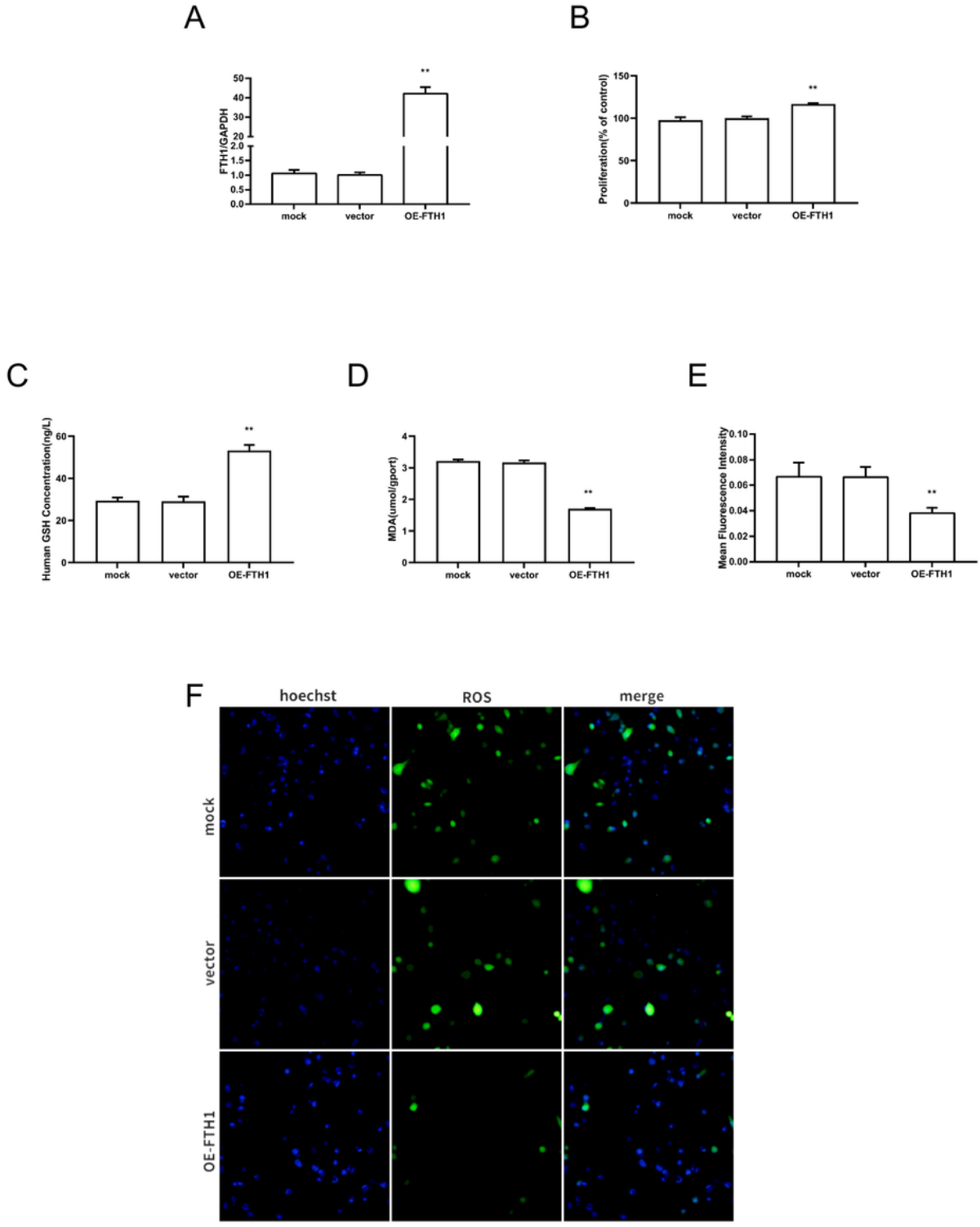

Figure 11

FTH1 mediated proliferation and ferroptosis in MGC803 cells. (A) MGC803 cells were transfected with FTH1 overexpression plasmid vectors(OE-FTH1) or empty vector. The transfection efficiency was validated using qRT-PCR. (B) The effect of FTH1 overexpression on cell viability was determined using the MTT assay. Mock, vector or OE-FTH1 group were measured the intracellular GSH level(C), the amount of MDA (D) released into culture medium, and ROS level(E, F) respectively. Hoechst 33342 was used

to identify Cell nuclei (blue), and ROS was used to detect intracellular reactive oxygen species levels (green). (original magnification, ×20) . *p < 0.05; **p < 0.01 versus vector. All data are representative of at least 3 independent experiments.